CFD Modeling of boron removal from liquid silicon with cold gases and plasma

Mathieu Vadon [1*], Øyvind Sortland [2], Ioana Nuta [1],
Christian Chatillon [1], Merete Tansgtad [2], Guy Chichignoud [1], Yves Delannoy [1]
*

[†1]SIMAP , [2] NTNU Department of Materials Science and Engineering
[*]Corresponding author: mathieu.vadon@simap.grenoble-inp.fr

Abstract

The present study focuses on a specific step of the metallurgical path of purification to provide solar-grade silicon: the removal of boron through the injection of $H_2O(g)$-$H_2(g)$-$Ar(g)$ (cold gas process) or of Ar-H_2-O_2 plasma (plasma process) on stirred liquid silicon. We are proposing a way to predict silicon and boron flows from the liquid silicon surface by using a CFD model (©Ansys Fluent) combined with some results on one-dimensional diffusive-reactive models to take into account the formation of silica aerosols in a layer above the liquid silicon. The comparison of the model with experimental results on cold gas processes provided satisfying results, for cases with low and high concentrations of oxidants. This confirms that the choices of thermodynamic data of $HBO(g)$ and the activity coefficient of boron in liquid silicon are suitable, and that the hypotheses regarding similar diffusion mechanisms at surface for $HBO(g)$ and $SiO(g)$ is appropriate. The reasons for similar diffusion mechanisms need further enquiry. We have also studied the effect of pressure and geometrical variations in the cold gas process. For some cases with high injection flows, the model slightly overestimates the boron extraction rate, and the overestimation increases with increasing injection flow. A single plasma experiment from SIMaP (France) was modelled and the model results fit the experimental data on purification if we suppose that aerosols form, but it is not enough to conclude on the formation of aerosols for plasma experiments.

I. INTRODUCTION

Solar grade silicon for photovoltaic cells has less purity requirements than electronic grade silicon [1]. This creates a need for exploration of new processes which are consuming less energy than processes from the chemical route for electronic grade silicon such as the Siemens process. Whereas the chemical route transforms the metallurgical-grade silicon (MG-Si) to be refined into gaseous species, the metallurgical route is made from a set of steps that extract the impurities from the MG-Si in its solid and liquid states.

Within the metallurgical route, solidification processes cannot remove boron efficiently because the segregation coefficient of boron is close to one. This is why another process is needed to remove boron. One category of processes [2] involves an impurity absorbing slag, another category involves the injection of cold gases or plasma with hydrogen and oxygen atoms, onto electromagnetically stirred and heated liquid silicon. Regarding the cold gas and plasma processes, the goal is to

[*]SIMAP, 1340, rue de la Piscine, 38402 Saint-Martin d'Heres, France
[†]NTNU Department of Materials Science and Engineering, Alfred Getz vei 2,7034 Trondheim, Norway

optimize the efficiency in the choice of the geometry, injection flow rate, composition of the injected mixture and silicon temperature. Computational fluid dynamics (CFD) simulations enable a better comprehension of the gas and plasma boron removal processes thanks to parametrical study and comparison to experiments, which will be the subject of this paper. The presented CFD simulations can also enable evaluation and optimization of these processes in different settings.

The CFD simulations were realized with ©Ansys Fluent (with extensions for the plasma process) , and have been used to model experiments by Sortland [3] and Altenberend [4]. First, we present the modelled experiments. Then we describe a one-dimensional model to estimate the effect of formation of silica aerosols on the flow of oxidant towards the surface and on the silicon oxidation rate. The boron removal rate is deduced from this oxidation rate using an equilibrium condition at the liquid surface and a simple model to compare the diffusion rate of boron and silicon, and their rate of condensation into silica aerosols. The thermodynamic data used for equilibrium will be justified and some possible explanations of the unity factor in the diffusion/precipitation model will be discussed. Then we compare the calculated silicon oxidation rate with the experimental silicon oxidation rate, and we compare the calculated and experimental boron purification rate. Extrapolating the model, we explore the effect of varying the crucible width or the total pressure. We discuss these results regarding the validity of chosen data and the CFD model, and also regarding the structure of the gaseous boundary layer.

II. PRESENTATION OF THE EXPERIMENTS

Cold gas Experiments of purification

We have modeled two sets of gas experiments with cold gas injections from Sortland [5] [3]. The two sets of experiments have a common geometry (Figures 1) and 2).

The first set of experiments is the Q_X experiment series, where a H_2-H_2O mixture of constant composition is injected at varying flows. The parameter controlled in the experiments is a total molar flow rate expressed in normal liters per minute (L_N/min), where 293 K is the reference temperature for normal liters. Geometrical parameters are given in 2 and other non-varying parameters are: Si(l) surface temperature of 1773 K, partial pressures of steam and hydrogen of $P_{H_2O} = 0.038$ bar and $P_{H_2} = 1.08$ bar at injection.

The values of input parameters that vary between the experiments, such as the molar flow, the durations of experiments, and the initial concentrations of boron are given in Table 1. The results such as the final concentrations and the total mass transfer coefficient (k_t) are also reported in Table 1. The total mass transfer coefficient defined in equation 1 is a measure for the kinetics of the process, independent of concentrations (c) and melt volume (V). It is however found to depend on the silicon surface area (A) due to varying conditions over the surface [3].

$$k_t = -\frac{\frac{\partial c_B(t)}{\partial t}}{c_B(t)} \frac{V}{A} \tag{1}$$

In the second set of experiments, H_2O_X , an Ar-H_2O mixture is injected. Only the partial pressure of H_2O(g) at injection is varying (see Table 2). The non-varying parameters are: Si(l) surface temperature of 1973 K and total gas inflow of 2 L_N/min. The concentration of oxidant at injection and the silicon surface temperature are much higher than for the Q_X experiments.
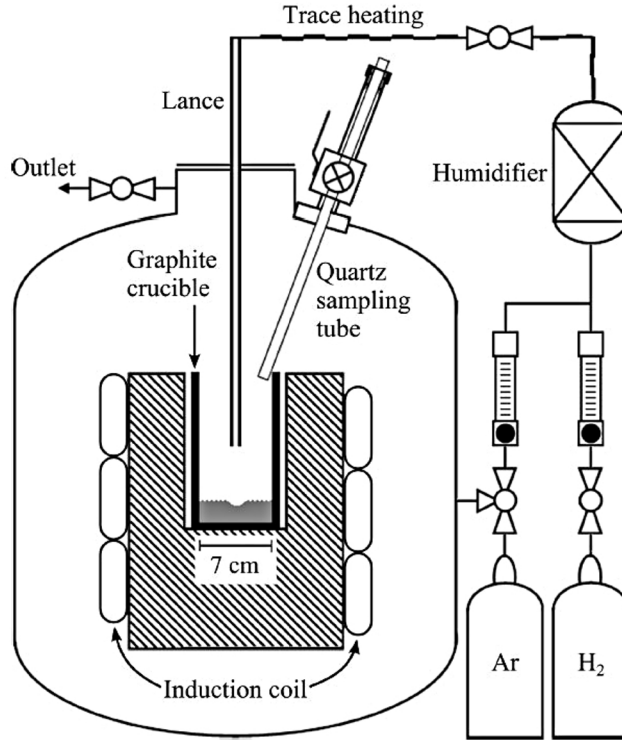
2

Figure 1: *Configuration of the modeled cold gas experiments. Source: Sortland [3].*

Plasma experiment

Figure 3 is representing the MAIA plasma experiment [4] [6], where a mixture of Ar-O_2-H_2 is inductively heated until the plasma state. This is a thermal plasma where the temperature inside the torch is over 10000 K [4]. The different experimental parameters are described in Tables 3 and 4.

III. IMPACT OF AEROSOLS ACCORDING TO THE ONE-DIMENSIONAL MODEL

Isothermal model

To describe the gas-side boundary layer, we are using a stagnant layer model developed by Vadon et al [7]. It assumes thermodynamical equilibrium and uniform temperature (T) equal to the silicon surface temperature. We also suppose zero net flow of oxygen atoms at the surface. Based on this model, we find the following silicon molar flux density (J_{Si}), which measures the oxidation rate (more details in annex A). D represents diffusion coefficients, δ is the boundary layer thickness and R is the universal gas constant.

$$J_{Si}^{heterogeneous} \approx \frac{D_{H_2O}P_{H_2O}^0 + D_{SiO}P_{SiO}^{surf}}{2\delta RT} \tag{2}$$

In the case without aerosols, the silicon molar flux density from the surface would be written

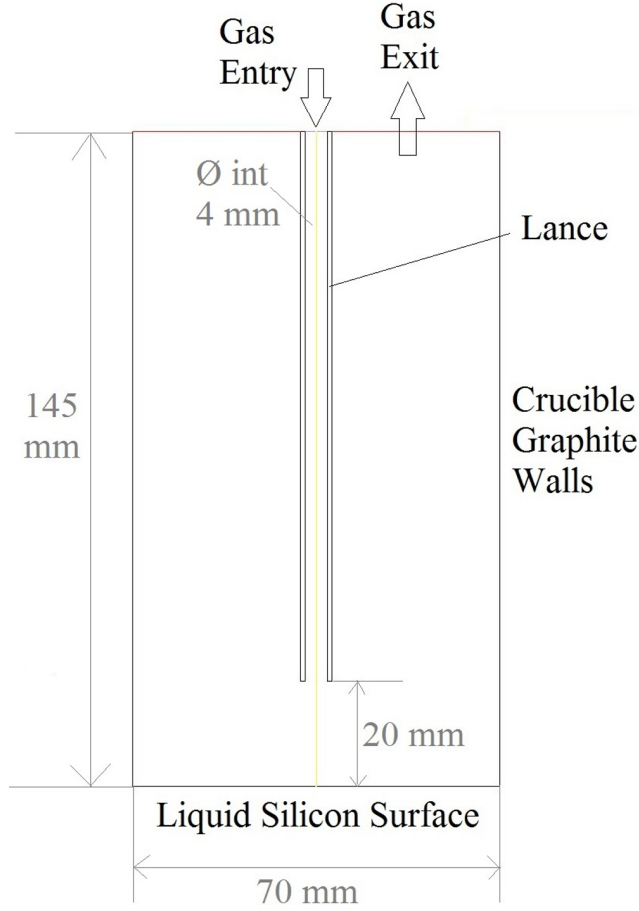**Figure 2:** *Crucible representation in the CFD model.*

using the conservation of oxygen atoms and equating the diffusive flows of SiO(g) and H_2O(g):

$$J_{Si}^{homogeneous} \approx \frac{D_{H_2O} P_{H_2O}^0}{\delta RT} \tag{3}$$

This leads to a ratio:

$$\frac{J_{Si}^{heterogeneous}}{J_{Si}^{homogeneous}} = \frac{D_{H_2O} P_{H_2O}^0 + D_{SiO} P_{SiO}^{surf}}{2 D_{H_2O} P_{H_2O}^0} \tag{4}$$

We have also made a simplified one-dimensional model that neglects the SiO_2(g) and O_2(g) species, thus keeping only SiO(g),H_2O(g),H_2(g),SiO_2(s/l) as species. This leads to the formula for the adimensionalized partial pressure of SiO(g) at surface:

$$p_{SiO}^{surf} = 2 \left(\frac{\Psi_{H_2O} p_{H_2}^{eff,0}}{K_{nuc} \Psi_{SiO} \Psi_{H_2}} \right)^{1/2} \tag{5}$$

where K_{nuc} is the equilibrium constant for the reaction SiO(g)+H_2O(g) $\leftrightarrows$ SiO_2(s/l)+H_2(g) of formation of silica aerosols, $p_{H_2}^{eff,0}$ (defined in annex A) is an adimensionalized effective hydrogen
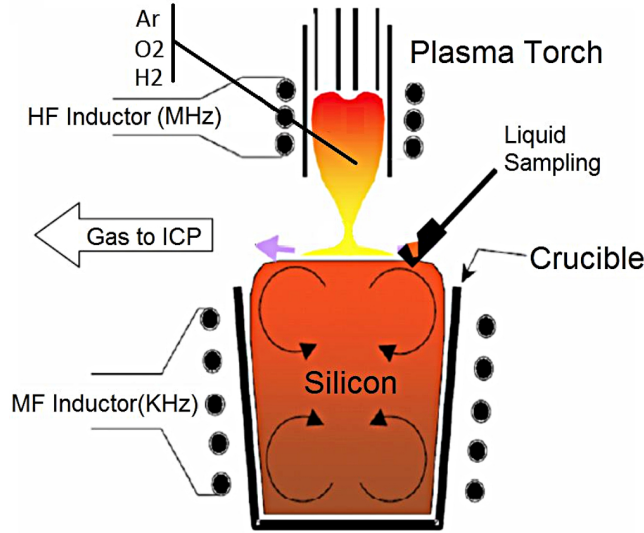
4

Figure 3: *Installation of the MAIA plasma configuration (source Altenberend [4]).*

97 partial pressure in the feeding gas, and $\Psi_X = D_X / D_{O_2}$ is the non dimensional diffusivity of species
98 X.

99 For the experimental range of temperature and hydrogen effective pressure considered in this
100 paper, the partial pressure of SiO at the surface, given by 5 is negligible compared to the water
101 vapor pressure out of the layer (see Table 5, whereas the diffusion coefficients of SiO and H_2O are of
102 the same order. Therefore, equation 4 simplifies to:

$$\frac{J_{Si}^{heterogeneous}}{J_{Si}^{homogeneous}} \approx \frac{1}{2} \tag{6}$$

103 **Non-isothermal model - cold gases**

104

105 We show in annex C, that if we suppose a negative temperature gradient from the surface (real
106 experimental case with cold gases), the equation 6 remains valid.

107 Furthermore, the formula 5 remains valid, except that it is using K_{nuc} at a lower temperature,
108 which reduces P_{SiO}^{surf}. The temperature decrease leads to more precipitation of silica aerosols, with
109 lower partial pressures of $H_2O(g)$ and SiO(g) inside the gaseous boundary layer compared to the
110 isothermal case. This reduces the concentration of oxidant at surface. Thus, the value of P_{SiO}^{surf}
111 should be lower than the value in equation 5, which makes the approximation 6 even more precise.
112 This is shown in Annex C. The real silicon flows can then be estimated by dividing the silicon flows
113 obtained by a CFD simulation without silica aerosols by two. Such a model will be validated in the
114 following sections, comparing half the silicon oxidation rate predicted by the CFD model to the
115 experimental oxidation rate.

116   IV.   DATA AND MODEL CHOICES

117 **Modeling options for the CFD model (Cold Gas)**

We are using an axisymmetric stationary laminar model taking into account mass (convection, diffusion) and heat transfer phenomena (convection, diffusion and radiation). Dirichlet boundary conditions are used in the CFD domain: ((see Figure 2): 1773 K (Q_X series) or 1973 K (H$_2$O_X series) around the silicon melt (liquid-gas and liquid crucible interface). The temperature of the crucible takes into account the conductivity of graphite for other areas of the crucible. The induction equations for the melt and the crucible are not included in the model and are replaced by these Dirichlet conditions. The temperature at the exit boundary is taken to be 1273 K, but has no influence on the transport because the convection is dominant for heat and mass transport at exit (see Figure 2) (the recirculations have little impact). The temperature of water vapor at injection up the crucible is taken to be 373 K, but the model has also little sensitivity to this parameter.

We chose to model only the gas phase, while supposing uniform temperature and concentration in the liquid silicon phase. Regarding the cold gas experiments, Sortland [3] studied the effect of stirring the liquid silicon by comparing similar experiments with 2 L$_N$/min gas flow rate in furnaces with different induction frequencies (4 kHz and 11 kHz). The different induction frequencies did no show an effect in the total mass transfer coefficient. At the highest gas flow rate of 16 L$_N$/min, simulations by Sortland [3] have also shown that the transport of boron in the liquid phase was non limiting.

The following equations were solved in ©Ansys Fluent, in stationary conditions for a single phase, for 2D axisymmetric geometries with isotropic diffusivities.

Mass conservation equation :
$$\nabla.\left(\rho\vec{v}\right) = 0 \tag{7}$$

Momentum conservation ($\vec{F}$ is the external forces, in our case gravity abd I is the unity matrix):

$$\nabla.\left(\rho\vec{v}\vec{v}^T\right) = -\nabla p + \nabla.\left[\mu\left(\nabla\vec{v} + \nabla\vec{v}^T\right) - \frac{2}{3}\nabla.\vec{v}I\right] + \vec{F} \tag{8}$$

Species transport:

$$\nabla.\left(\rho\vec{v}Y_i\right) = -\nabla.\vec{J}_i + R_i \tag{9}$$

where R_i is the net rate of production of species i by chemical reaction, Y_i the mass fraction of species i. J_i is the diffusive flow (in kgm^{-2}s^{-1}). Its expression is given in laminar conditions and for an ideal gas at constant pressure by a component taking into account the mass fraction gradients and the thermodiffusion component. The choice for the laminar model was made after the comparison for the experiment with the highest rate (Q_16a) had shown that the introduction of the $k - \omega$ SST model made no significant difference in the results.

J_i is the solution of the equation of Maxwell-Stefan with a term that includes the thermodiffusion component:

$$\sum_{j=1,j\neq i}^{N}\frac{X_iX_j}{D_{ij}}\left(\frac{\vec{J}_j}{\rho_j} - \frac{\vec{J}_i}{\rho_i}\right) = \nabla X_i - \frac{\nabla T}{T}\sum_{j=1,j\neq i}^{N}\frac{X_iX_j}{D_{ij}}\left(\frac{D_{T,j}}{\rho_j} - \frac{D_{T,i}}{\rho_i}\right) \tag{10}$$

where X_i is the mole fraction, T the temperature in K, D_{ij} the binary mass diffusivity of i in j (in m^{2}s^{-1}), $D_{T,j}$ the thermal diffusion coefficient of j. The binary mass diffusivities are calculated from the lennard-jones parameters and the temperature, and the thermal diffusion coefficien from the molecular masses and the temperature.

6

The energy equation is written for the specific energy E of the mixture, with viscous heating being neglected:

$$\nabla.\left(\vec{v}\left(\rho E + p\right)\right) = \nabla.\left(k_{eff}\nabla T - \sum_j h_j \vec{J}_j\right) + S_h \tag{11}$$

The first term on the right represent heat conduction (k is the thermal conductivity) and the second term is heat transport by species diffusion (h_j is the specific enthalpy of species j). S_h includes the volumetric heat of reaction. The model does not contain volumetric reactions, so this term equals zero.

The radiation model is a surface-to-surface model (that is the gases are transparent to radiations), where the surfaces are represented as black bodies.

The integration method used the ISAT tables. In this method, tables store calculated values on different points. New values are calculated by using previously stored values of points with input parameters that approximate those of the point for which the calculation is being performed (Ansys Manual [8] and S.B.Pope [9]).

Modeling options for the CFD model (Plasma)

The CFD model for plasma has many similarities to the model for cold gases. It is axisymmetric and supposes uniform temperature and concentrations in the liquid. Delannoy et al. [10] has shown that for a similar setting in a cold crucible, the characteristic time after which the concentration of boron is reduced by a factor $e = 2.71$ was about 2 min if taking into account only the transfer in the liquid phase while the experimental characteristic time is about 90 min in Altenberend [4].

The model also uses the ISAT algorithm. The CFD model used for the plasma experiment is taken from Pelletier et al. [11] and Majchrzak et al. [12]. This model also uses the equations of momentum, energy and mass conservation previously described. Additionally, in these equations, this model takes into account the induction forces inside the plasma torch, the Joule effect of the currents inside the plasma, and the kinetics of formation of species such as ion and radicals.

Contrary to the cold gas model, it also includes turbulence modelling. For the turbulence, the $k - \omega$ SST turbulence model was used using options from Ansys Fluent. This model introduces a turbulent kinetic energy term k and a specific turbulence dissipation rate ω, using statistical moments of turbulent fluctuations. to solve the equation of conservation of moment. Compared to laminar terms for mass and heat transport, this leads to additional terms of turbulent diffusivities.

Some specific modules have been programmed by Pelletier et al. [11] and Majchrzak et al. [12] to determine the mass fractions of the different species which include radicals and ions. Due to the high temperatures, we suppose that the plasma is at the same temperature for all the species (thermal plasma). We suppose that the energy distribution levels follow the Boltzmann law. The kinetics of formation of ions and radicals follow a Arrhenius law. The Arrhenius parameters are described in Table 8, 9 and 10.

Regarding induction, some specific modules have been programmed by Delannoy and are described in Pelletier et al. [13]. They solve the Lorentz equations (magnetic force on the charged particles) and the joule effect, and integrate them in the momentum and energy conservation equations.

The plasma emits and absorbs radiation. In order to obtain a better calculation speed, a simplified model has been used where the plasma is optically transparent (so it doesnt't absorb any radiation). The heat is lost through a term depending on the local temperature and the local composition, using net emission coefficients tabulated by the National Institute of Standard and Technology [1] using a model and files from Lacombe [14].

Degoulange [15] found by simulations with a graphite crucible that the plasma heated the surface by a maximum of 10 K. The information for this simulation is reported in Tables 3 and 4. The conditions seem to be of the same order. The distance from the torch to the surface is 60 mm in the experiment by Altenberend, which favors more heating of the surface compared to a simulation by Degoulange with 100 mm torch distance. However, the experiment by Altenberend is made in a cold crucible and the experiment by Degoulange [15] in a graphite crucible. A cold crucible is letting more of the magnetic field inside the melt than a graphite crucible because solid silicon is less conductive than graphite, which should improve the stirring in the cold crucible. Hence it is likely that the local overheating of the surface of the liquid silicon doesn't have an important role regarding the plasma experiment by Altenberend.

Preliminary results on equilibrium at surface

Alemany et al.[16] and Sortland [3] have both confirmed that the dominant species including boron in the gas phase is HBO(g). JANAF data shows that SiO(g) is the only major species with silicon atoms in the gas phase (Sortland [3]). Altenberend [6] has show that an equilibrium exists at the surface between HBO(g), SiO(g), Si(l) and B(in Si) for liquid silicon under an oxidizing thermal plasma. This implies that the enrichment factor Rf, defined in 12, can be calculated by the second part of 12. [i] denotes the concentration of species i.

$$
\begin{aligned}
Rf &= \frac{([B]/[Si])_{surf,gas}}{([B]/[Si])_{liquid}} \\
Rf &\approx \gamma_B K p_{H2}^{1/2}
\end{aligned}
\tag{12}
$$

Where :

- K is the equilibrium constant of the reaction $SiO(g) + \frac{1}{2} H_2(g) + B(in\ Si) \leftrightarrows Si(l) + HBO(g)$

- γ_B is the infinite dilution activity coefficient of B in Si(l)

Considerations on the η factor

We define the factor η as the ratio of silicon flow and boron flow from the reactive surface divided by the enrichment factor Rf. The definition of the enrichment factor comes from Altenberend et al. [6]. This takes into account the different ways the gaseous boron and silicon species are diffusing from the surface. The formation of silica aerosols may impact the diffusion of boron and of silicon differently. All the same, there may be differences in diffusivities of HBO(g) and SiO(g).

$$
\begin{aligned}
\eta &= \left(\frac{J_B}{J_{Si}}\right) / \left(Rf\frac{[B(\ in\ Si)]}{[Si(l)]}\right) \\
&\approx \left(\frac{J_B}{J_{Si}}\right) / \left(\frac{P_{HBO}}{P_{SiO}}\right)
\end{aligned}
\tag{13}
$$

---

[1] http://physics.nist.gov/PhysRefData/ASD/lines_form.html

Presentation of the different methods for estimating purification and oxidation rates

In this section, we are presenting two ways for estimating purification and oxidation rates, one better adapted for low concentrations of $H_2O(g)$ at injection, and the second for higher concentrations of $H_2O(g)$ at injection.
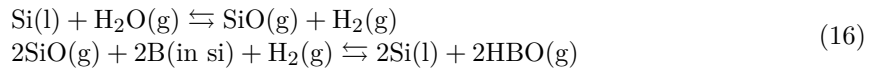
There are two reactions for silicon oxidation [2] The reaction 14 has a dilution effect because one mol of gas reactant produces two mol of gasseous products. The reaction 15 on the contrary has a concentration effect.

$$Si(l) + H_2O(g) \leftrightarrows SiO(g) + H_2(g) \tag{14}$$

$$SiO(g) + H_2O(g) \leftrightarrows SiO_2(s/l) + H_2(g) \tag{15}$$
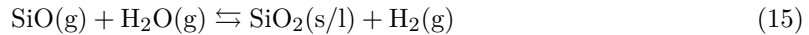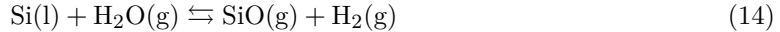
Method A

In this method, the species $SiO(g)$, $HBO(g)$, $H_2O(g)$, $H_2(g)$, $Si(l)$,$B(in\ Si)$,$Ar(g)$ are included in the CFD model. The SiO flow and the HBO flow are divided by two to take into account the formation of silica aerosols, which are not modelled in the CFD code.

The reactions included are surface reactions (liquid silicon oxidation and purification reaction below) but no volumic reaction has been included.

$$\begin{aligned} Si(l) + H_2O(g) &\leftrightarrows SiO(g) + H_2(g) \\ 2SiO(g) + 2B(in\ si) + H_2(g) &\leftrightarrows 2Si(l) + 2HBO(g) \end{aligned} \tag{16}$$

This method is adapted only for low concentrations of oxidant at injection, where phenomena of dilution and concentration are not significant. The reason is that in the CFD model, dilution phenomena from the surface oxidation are included in the model but not the concentration phenomena from the volumic reaction of oxidation of $SiO(g)$ to form silica.

Method B

In this method, only the species $H_2O(g)$, $H_2(g)$, $Ar(g)$ are included in the model, as well as a fictive species $H_2'(g)$ which has the thermodynamic properties of $H_2O(g)$ and the diffusivity properties of $H_2(g)$. The silicon flow is calculated by estimating the flow of $H_2O(g)$ towards the surface, which is given by the outflow of the fictive species $H_2'(g)$, then this flow is divided by two to take into account the nucleation and growth of silica aerosols. This model supposes that the dilution by reaction 14 and concentration in equal proportions by reaction 15 happen very close to the surface. Since $H_2(g)$, a product of both reactions, has a high diffusivity, the concentration and dilution compensate each other and thus have no significant influence on the transport of oxidant towards the surface. We still have to divide the calculated flow of $H_2(g)$ by two because half of the H_2O molecules in the model that react with $Si(l)$ to form $H_2(g)$ have first reacted with $SiO(g)$ above the silicon surface. This model is well adapted for high concentrations of oxidant because it takes both self compensating phenomena of dilution and concentration into account, which is not the case of model A.

---

[2]In annex A we show that the hypothetical appearance of Si(OH)4 should not affect the flow of silicon and oxygen towards the surface.

The boron flow is calculated with the following steps:

1. Calculate the local $H_2O(g)$ flow at the surface, which is purely diffusive to estimate the local flow of silicon.

2. Calculate the local partial pressures $P_{H_2} + P_{H_2'}$ at surface as an estimate of P_{H_2} at surface.

3. Use the local values of the enrichment factor Rf calculated with the estimated value of P_{H_2} at surface, and multiply it by the concentration of boron in the liquid and the local flow of silicon at the surface to get the local flow of boron.

Contrary to method A, method B is valid for higher concentrations of oxidants at injection. Method B is also valid for the lower concentrations. If a margin of error of 5% for instance is tolerated, a concentration of $H_2O(g)$ that is less than 5% is considered a low concentration and method A can be used. We remind that about half of the $H_2O(g)$ molecules react to form silica aerosols, leading to a dilution of one mol per mol of $H_2O(g)$ reacting with $SiO(g)$ to form silica aerosols. Thus in that case, supposing that the concentration of $H_2O(g)$ is of the same order as in the injection [3], the effect of dilution is less than 5%. However, we will see that for low concentrations there is only a small difference in the results between method A and method B.

The advantage of Model A over Model B is that Model B supposes that $\eta = 1$ where as model A takes into account the diffusivities of $HBO(g)$ and $SiO(g)$ within the configuration of a laminar impinging jet. However the uncertainties on the diffusivity of $HBO(g)$ are big, while the differences between the two models were shown to be small for a case at low concentration. The comparison of the mole fraction of oxidant at injection to the tolerated margin of error can help to say if method A can be implemented. In case of doubt about whether the concentration of oxidant is low enough, it is a better to use method B which is valid for all ranges of concentrations.

Method for the plasma

The CFD model for plasma does not include surface reaction products such as $SiO(g)$ and $HBO(g)$. The flows of $SiO(g)$ and $HBO(g)$ are instead calculated indirectly, assuming $\eta = 1$. The flow if $SiO(g)$ is calculated from the flow of oxygen atoms in species with oxygen (mainly H_2O,OH and O). The local concentration of H_2 on the surface is calculated using the local concentrations of H_2 and of the radical H. The hydrogen that would result from the oxidation of silicon by H_2O is not taken into account. Given the dependence of the enrichment factor on hydrogen as $Rf \propto \left(p_{H2}^{surf} \right)^{1/2}$, this leads to a gross underestimation of the boron flow of about $1 - \left(\frac{x_{H2}^0 - 2x_{O2}^0}{x_{H2}^0} \right)^{1/2} = 1 - \left(\frac{0.031 - 2 \times 0.06}{0.031} \right)^{1/2} \approx 22\%$.

Choice of the thermodynamical values

The thermodynamical values for $SiO(g)$,$Si(l)$,$H_2(g)$, $H_2O(g)$ in the model have been chosen from JANAF [17]. However proper thermodynamical values for $HBO(g)$ and the activity coefficient of boron in liquid silicon, necessary to know the value of the enrichment factor Rf, had to be selected in other ways.

---

[3]in reality the concentration of H2O(g) is probably lower near the surface than at injection because Ar and $H_2O(g)$ have similar diffusivities and some of the $H_2O(g)$ has already reacted

Choice of the standard enthalpy of formation of HBO(g)

The data on the standard enthalpy of formation of HBO(g) available in the litterature vary widely, which causes even greater variations for the rate of the purification process. Using refining experiment results from Sortland [3], it appears that the enthalpy of formation of HBO(g) is necessarily lower than -248 kJ/mol. Thus, the only compatible values for the enthalpy of formation of HBO(g) found in the litterature, are the values from Page [18] resulting from ab initio calculation and the experimental value from Gorokhov [19], updated with experimental values of B_2O_2 from Jacobson [20]. The value from Page is -251 kJ/mol. The initial value from Gorokhov et. al. is $\Delta_f H_{\mathrm{HBO(g)}}(0\ \mathrm{K}) = -228$ kJ/mol. It is deduced from mass spectrometer measurements for the reaction $B_2O_2(g) + HBO_2(g) \leftrightarrows B_2O_3(g) + HBO(g)$. We change the initial value from Gurvich [21] $\Delta_f H_{\mathrm{B_2O_2(g)}}(298.15\ \mathrm{K}) = -457.7$ kJ/mol with the new value from Jacobson [20] $\Delta_f H_{\mathrm{B_2O_2(g)}}(298.15\ \mathrm{K}) = -479.9$ kJ/mol. Given that the initial value from Gorokhov [19] for HBO(g) is $\Delta_f H_{\mathrm{B_2O_2(g)}}(0\ \mathrm{K}) = -228$ kJ/mol, the new corrected value is $\Delta_f H_{\mathrm{HBO(g)}}(0\ \mathrm{K}) = -250.2$ kJ/mol. Then using the calorific capacity from Gurvich, this leads to $\Delta_f H_{\mathrm{HBO(g)}}(298.15\ \mathrm{K}) = \Delta_f H^0_{\mathrm{HBO(g)}} = -250.8$ kJ/mol.

$$\Delta_f H^0_{\mathrm{HBO(g)}}(298.15\ \mathrm{K}) = -250.8\ \mathrm{kJ/mol} \tag{17}$$

Choice of the molecular entropy of HBO(g)

Regarding the entropy, we take the value from Gurvich [21] of $S^0_{\mathrm{HBO(g)}}(298.15\ \mathrm{K}) = 202.691$ kJ/mol.

Choice of the activity coefficient of boron in liquid silicon

Given the typically low concentrations of boron in MG-Si (less than 1 ppm [1]) and the low concentrations of boron in the experiments (typically 30-50 ppm), we can approximate the activity coefficient of boron with the infinite dilution coefficient. The most reliable value appears to be that from Freis et Lukas (in COST21 [22]) because it converges towards one when the temperature increases, thus approaching the behaviour of an ideal solution. These value results from an optimization.

$$log_{10}(\gamma_B^\infty) = 1105/T - 0.1105 \tag{18}$$

Thus the estimated values of γ_B, $H_{f,\mathrm{HBO(g)}}$ and $S^0_{\mathrm{HBO(g)}}$ enable us to represent the enrichment factor Rf on the surface (equation 12) in Figure 4, assuming $P_{\mathrm{H_2}} = 1$ bar.
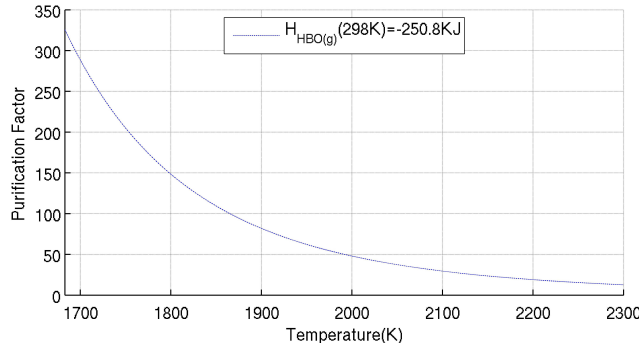

Figure 4: *Reduced enrichment factor $\gamma_B K = \frac{Rf}{p_{H2}^{1/2}}$ as a function of liquid silicon temperature, assuming $P_{H_2} = 1$ bar.*

11

Estimation of diffusivities

The diffusivities are calculated using the Lennard-Jones formula. The Lennard-Jones parameters for HBO(g) are not available in the litterature. However using empirical rules as well as data on H_2, B_2, O_2, H and BO from Svehla [23], we come to a first estimation of $\epsilon/k = 596$ K and $\sigma = 3.081$ Å

V. Simulation Results

Comparison of mass losses between model and experimental results: Q_X series

Figure 5 shows that model A can very well predict the silicon oxidation rates for the high dilution series of experiments Q_X .
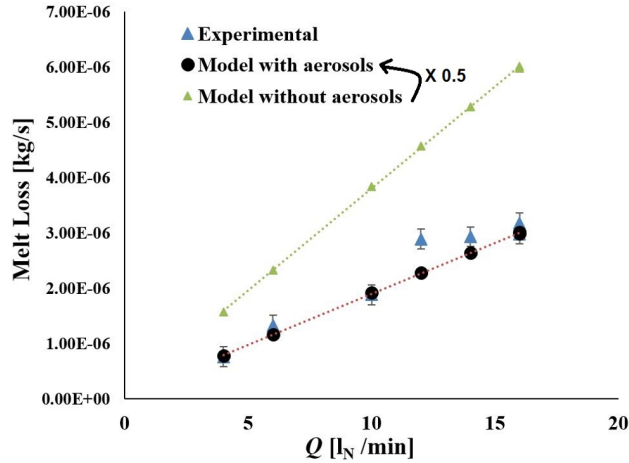

Figure 5: *Comparison of the silicon flows for the experiment series Q_X from Sortland [5] between experimental results and model.*

Comparison of purification rates between model and experimental results: Q_X series

Model A was used for the estimation of purifications rates for Q_X series with high dilution (Figure 6). The results show good agreement between simulated values and experimental values for purification rates despite a small overestimation. At the higher injection flows (14 and 16 L_N/min) there is an increasing divergence between experimental and predicted purification rates. However, the modeled purification rates with high injection flows appears coherent with simulated values at lower injection flows.
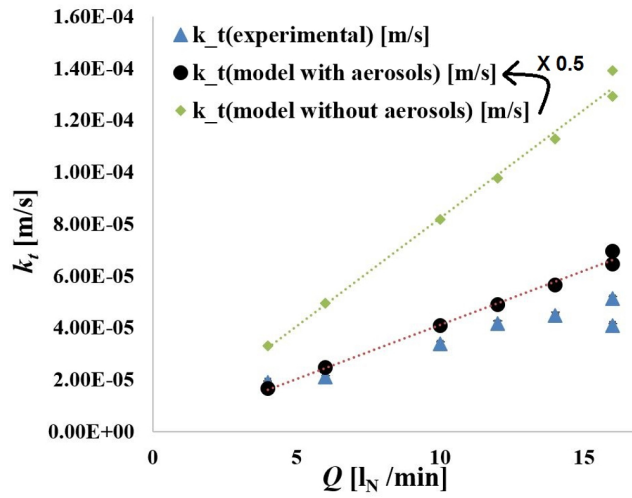
12

Figure 6: *Comparison of total mass transfer coefficients k_t for the experiment series Q_X between experimental results and model*

Comparison of purification rates between model and experimental results: H_2O_X series

Model B was used for the estimation of purifications rates for H_2O_X series with high concentration of oxidant (Figure 7). The results show good agreement between simulated values and experimental values for purification rates despite a small underestimation. This validates the model B and the hypotheses that dilution and concentration of reactions 14 and 15 happen sufficiently close to the surface to neutralize each other. Model B was also tested for experiment Q_16a with high dilution of $H_2O(g)$ at injection. There was 5% of difference in purification rate compared to the results of model A (point not represented).
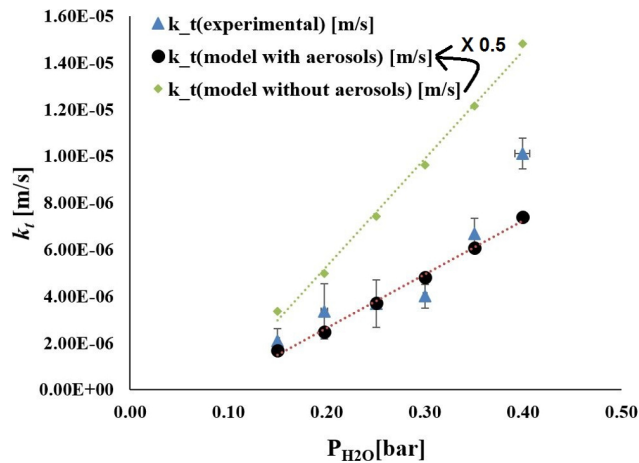

Figure 7: *Comparison of total mass transfer coefficients k_t for the experiment series H_2O_X between experimental results and model*

Influence of total pressure: Q_X series

³³⁸ For the hydrogen rich Q_16a experiment series, the simulation (model A) shows that an increase
³³⁹ of total pressure is increasing the purification rate (represented by k_t as a square root of the total
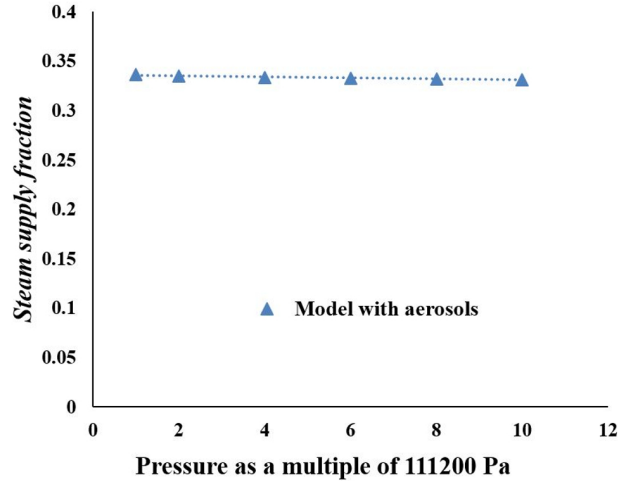³⁴⁰ pressure, all other things being equal.

Figure 8: *Steam supply fraction (SSF) as a function of total pressure with the parameters of Q_16a experiment*

³⁴¹ **Influence of a wider crucible: Q_X series**

³⁴² For the experimental conditions of the Q_16a experiment (model A) , an increase of the crucible
³⁴³ diameter should have only little effect on the purification rate according to the simulations. In
³⁴⁴ Figure 9, the steam supply fraction, defined as the fraction of $H_2O(g)$ that reaches the surface to
³⁴⁵ form $SiO(g)$ increases only little when the crucible becomes wider.
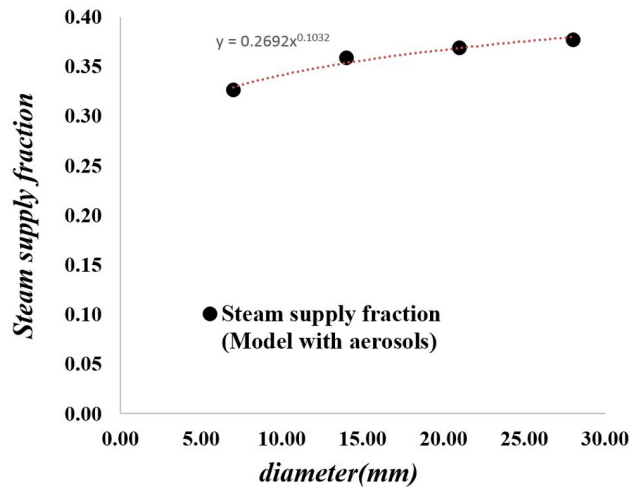

Figure 9: *Steam supply fraction (SSF) as a function of crucible diameter Q_16a*

³⁴⁶ **Temperature profile in plasma and impact on nucleation**

³⁴⁷

14

Using values from [24] at 1 bar, the maximum temperature at which silica is thermodynamically stable is 3139 K. This is the maximum temperature value for an optimal ratio of silicon over oxygen atoms. The temperatures of vaporization is lower for other concentration ratios of silicon and oxygen atoms. The maximum thickness of the layer above the liquid silicon surface at which silica is thermodynamically stable in condensed state is about $0.5 - 1$ mm for the majority of the surface (except very close to the walls). Furthermore, kinetics of nucleation and growth of silica aerosols can also be limiting. Hence there are good reasons to suspect that the formation of silica aerosols does not occur for plasma purification, but it can't be entirely excluded either if the silica particles are forming very close to the surface as suggested by the one-dimensional model at thermodynamical equilibrium (Vadon et al. [7]).
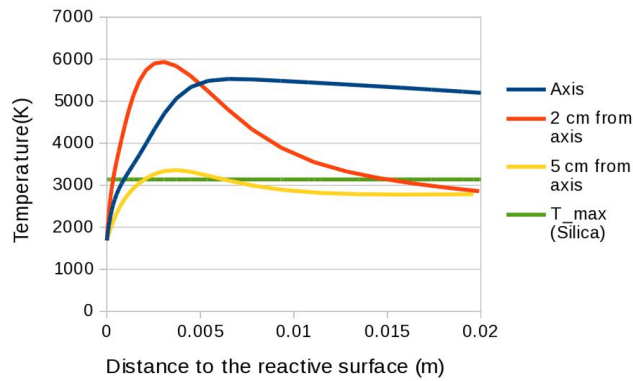
Figure 10: *Evolution of temperature in the gas phase between z=0 (liquid surface) and z=1 cm (1 cm from liquid surface) at different distances from symmetry axis*

Results on plasma

Regarding the plasma purification experiments, the CFD simulation that doesn't include nucleation gives $k_t = 3.31 \cdot 10^{-5}$ m/s, twice the experimental value of $k_t = 1.47 \cdot 10^{-5}$ m/s (Figure 11).

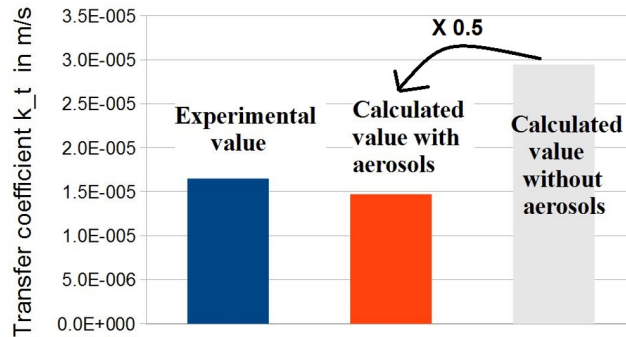**Figure 11:** *Total mass transfer coefficient for the plasma purification experiment compared to models with and without aerosols.*

15

VI. Discussion

Influence of the formation of silica aerosols on the oxidation rate

The good agreement between Q_X experiments and model A for the oxidation rate for cases with low concentration of oxidants at injection is confirming our results from the 1D model, that nucleation reduces the oxygen flow towards the surface by a factor two. Let us remark that for this approximation to hold true, it is just necessary to have $P_{\text{SiO}}^{surf} \ll P_{\text{H}_2\text{O}}^0$. We can have such a relationship without necessarily having thermodynamical equilibrium for the silica aerosols with the gas.

Effect of a high concentration of oxidant

The validation of model B for a good prediction of oxidation and purification rates for high concentrations of oxidants is all the more interesting since the 1D model supposed a high dilution of oxidants to be able to apply Fick Law. This shows that the hypothesis of formation of silica aerosols dividing by two the inflow of oxidants also applies in cases of high concentrations of oxidants.

Choice of thermodynamical data and of the η factor

The choice of the thermodynamical data seems quite accurate if we suppose $\eta = 1$. First let us remind that Sortland [3] has found out that the silica particles at the exit of the process are very rich in boron and that Altenberend [4] has shown that the boron contents in the fumes corresponds to what is extracted from the silicon. $\eta = 1$ would suppose that the precipitation of HBO(g) would be simultaneous with the formation of silica aerosols, with condensation rates proportionnal to their respective gas concentration. Further thermochemical studies would be necessary to assess this hypothesis, but they are difficult because of the nanometric size of the aerosols (which could modify their thermodynamic data), and because of their unknown nature (liquid of various solid phases are possible).

Case of chemical kinetics limitation of the purification reaction

The results on purification rates for experiment Q_16a in Figure (Figure 6) show that for high flows of injections, the model starts overestimating the purification rate. There can be several explanations for this. First, some kinetic limitation may appear for experiments Q_14, Q_16a and Q_16b . The chemical mechanism is not well known for the purification reaction. Possible limiting factors might be the absorption of hydrogen onto the liquid silicon surface or the formation of BO(g) at the liquid silicon surface that then would react with hydrogen to form HBO(g). Another explanation could be that the η factor would start changing at higher injection flows because of different kinetics of precipitation of HBO(g) and SiO(g) to form the silica aerosols enriched in boron.

Discussion on the plasma results

Regarding the simulation data for the plasma experiment from Altenberend [4], if the CFD model is correct, the thermodynamical data with $\eta = 1$ while supposing the presence of aerosols fit the results much better than if we suppose the absence of aerosols. This is all the more true in that the current model is underestimating the concentrations of hydrogen at surface which contributes to an underestimation of the boron flows. The problem however is that the thickness of the surface layer on which silica particles are thermodynamically stable is very thin. Since there is only a single

16

simulation compared to experiment, we can not draw conclusions. A local overheating of the surface under the jet that reduces the enrichment factor Rf is a possibility that was not taken into account by the model, which assumes an isothermal liquid. However, Degoulange [15] found that for similar conditions, the local heating of the silicon surface was less than 10K due to efficient stirring.

VII.   Conclusion and Perspectives

For gas processes aimed at extracting boron from liquid silicon, we developed models able to accurately predict the silicon oxidation rate and the purification rate. Thanks to theoretical considerations through a one-dimensional model and comparisons of a CFD model to experimental data, we show that the oxidation model has to take into account the formation of silica aerosols close to the surface, as this consumes half the oxidant diffusing towards the surface. The rate of boron extraction is correctly described by a chemical equilibrium at the interface and a simultaneous diffusion and condensation of SiO and HBO into silica particles. The reason for such a simultaneous formation of aerosols remains to be explained theoretically using thermodynamics adapted to nanoparticles and diffusion laws. Last but not least, our model was able to describe cold gas experiments as well as a plasma purification experiment, without any modification (including the aerosols layer, still needed in the plasma process).

VIII.   Aknowledgements

IX.   Notations

- D_X Diffusivity of species X

- P_X Partial pressure of species X

- p_X Dimensionless partial pressure of species X, taken as the value when expressed in bar

- $\Psi_X = D_X / D_{O_2}$

- J_X Flow of species or atom X in $mol/m^2/s$

- $P_{O_2}^{eff} = \frac{1}{2}\psi_{H_2O}P_{H_2O} + \frac{1}{2}\psi_{SiO}P_{SiO} + \psi_{SiO_2}P_{SiO_2}$ Effective pressure for oxygen

- $P_{Si}^{eff} = \psi_{SiO}P_{SiO} + \psi_{SiO_2}P_{SiO_2}$ Effective pressure for Si

- $P_{O_2}^{eff,surf}$ Effective pressure for oxygen at surface

- $P_{O_2}^{eff,ext}$ Effective pressure for oxygen at injection

- P_{Si}^{sat} Saturation pressure of Si(g) which is also the pressure of Si(g) at surface

- δ Thickness of the boundary layer

- c Total molar concentration of gas

- c_B Concentration of boron in the fluid

17

434   • x_B Mole fraction of boron in liquid

435   • K_{nuc} Equilibrium constant of the reaction $SiO(g) + H_2O(g) \leftrightarrows SiO_2(s/l) + H_2(g)$

436   • R: Universal gas constant

437   • Rf: Enrichment factor

438   • k_t: Total mass transfer coefficient

A.   Simplified 1D-Isothermal model

440 In this section, we are using the one-dimensional model by Vadon et al. [7] to reason why the silicon
441 outflow in diluted cases is half of what it would be if the nucleation of aerosols did not occur.

442   We consider a stagnant boundary layer of thickness δ, where the only reactive species are H_2O
443 ($P^0_{H_2O}$) and $H_2(g)$. Liquid silicon is at the reactive surface (z=0). As represented by Ratto [25]
444 and Vadon et al. [7], the boundary layer is made of a lower homogeneous sublayer (i.e. without
445 silica aerosols), an intermediate heterogeneous sublayer (equilibrium K_{nuc} of the reaction $SiO(g) +$
446 $H_2O(g) \leftrightarrows SiO_2(s/l) + H_2(g)$) and a homogeneous upper sublayer.
447   Hypotheses:

448   • Thermodynamical equilibrium everywhere.

449   • Net flow of oxygen and hydrogen atoms at surface equal to zero.

450   We define for this part the effective pressures, which are used to express the flow of oxygen and
451 silicon atoms as parts of gas molecules:

$$
\begin{aligned}
P^{eff}_{Si} =& \ \Psi_{Si}P_{Si} + \Psi_{SiO}P_{SiO(g)} \\
& + \Psi_{SiO_2}P_{SiO_2(g)} + \Psi_{Si(OH)_4}P_{Si(OH)_4(g)} \\
P^{eff}_{O_2} =& \ \tfrac{1}{2}\Psi_{H_2O}P_{H_2O} + \tfrac{1}{2}\Psi_{SiO}P_{SiO(g)} \\
& + \Psi_{SiO_2}P_{SiO_2(g)} + 2\Psi_{Si(OH)_4}P_{Si(OH)_4(g)} \\
P^{eff}_{H_2} =& \ \Psi_{H_2O}P_{H_2O} + \Psi_{H_2}P_{H_2} + 2\Psi_{Si(OH)_4}P_{Si(OH)_4(g)}
\end{aligned}
\tag{19}
$$

In Vadon et al, it is shown that because of the formation of silica aerosols in every point of the
layer, the quantity per time unit of oxygen atoms going from the gas phase to the silica phase is
twice the quantity per unit time of silicon atoms going from the gas phase to the silica phase. As a
result (index 0 means at injection):

$$
\begin{aligned}
P^{eff}_{O_2} - P^{eff}_{Si} &= Az + B \\
P^{eff}_{H_2} &= P^{eff,0}_{H_2}
\end{aligned}
\tag{20}
$$

452   Thus, by looking at the conditions at surface (z=0) and at the top of the boundary layer ($z = \delta$),
453 the molar flow per m^2 (J_{Si}), and using the hypothesis of a zero net oxygen flow from the surface:

$$
J_{Si} = -\frac{D_{O_2}}{RT}\frac{\partial P^{eff}_{Si}}{\partial z}(z=0) = \frac{D_{O_2}}{RT}A =
$$
$$
\frac{D_{O_2}}{RT}\frac{\Psi_{Si}P^{sat}_{Si} + \tfrac{1}{2}\Psi_{H_2O}P^0_{H_2O} + \tfrac{1}{2}\Psi_{SiO}P^{surf}_{SiO} - \tfrac{1}{2}\Psi_{H_2O}P^{surf}_{H_2O} - \Psi_{Si(OH)_4}P^{surf}_{Si(OH)_4(g)}}{\delta}
\tag{21}
$$

454   Then, using thermodynamical data from JANAF [17] , we can neglect $\Psi_{Si}P^{sat}_{Si}$ and $\Psi_{H_2O}P^{surf}_{H_2O}$.
455 They are small compared to $P^0_{H_2O}$, which is higher than 100 Pa in the studied cases.

18

456 Using data from Plyasunov et al. [26] (also cited in Opila et al [27]) for $Si(OH)_4$, we can
457 also neglect $P_{Si(OH)_4}$ in compararison to P_{SiO} at the surface, in presence of liquid silicon. At
458 thermodynamical equilibrium, in presence of $Si(l)$, $\frac{p_{SiO}^4 p_{H_2}^2}{p_{Si(OH)_4}} > 3 \cdot 10^6$ for $T > 1687\,K$ [4], when
459 pressures are expressed in bars. Thermodynamical data for $Si(OH)_4$ is presented in Table 7. In
460 the case the values of $P_{Si(OH)_4}$ were to get higher compared to P_{SiO} in other zones upwards the
461 boundary layer, this would be of no impact on the inflow of oxygen towards the surface and on the
462 outflow of silicon..

$$J_{Si} \approx \frac{D_{O_2}}{RT} \frac{\frac{1}{2}\Psi_{H_2O}P_{H_2O}^0 + \frac{1}{2}\Psi_{SiO}P_{SiO}^{surf}}{\delta} \tag{22}$$

463 This enables us to build a simplified model where only the species $Si(l)$, $SiO(g)$,$H_2O(g)$ are taken
464 into account. By using the conditions at the intersection of the homogeneous sublayer (zero flow of
465 oxygen atoms) and the heterogeneous sublayer like in Vadon et al. [7], we can thus find an analytical
466 expression of the partial pressure of $SiO(g)$ at the surface in equation 5.

467 ## B. DEPENDENCE OF RATIOS OF DIFFUSIVITIES ON TEMPERATURE

In Bird et al [29], the following equations are given for the binary diffusivity of i in j :

$$
\begin{aligned}
D_{ij} &= 0.00188 \frac{\left[T^3\left(\frac{1}{M_{w,i}} + \frac{1}{M_{w,j}}\right)\right]^{1/2}}{P_{abs}\sigma_{ij}^2\Omega_D} \\
T_D^* &= \frac{T}{(\epsilon/k_B)_{ij}} \\
(\epsilon/k_B)_{ij} &= \sqrt{(\epsilon/k_B)_i (\epsilon/k_B)_j} \\
\sigma_{ij} &= \frac{1}{2}(\sigma_i + \sigma_j) \\
\Omega_{D_{ij}} &= \frac{1.06036}{T^{*0.15610}} + \frac{0.19300}{exp(0.47635T^*)} \\
&+ \frac{1.03587}{exp(1.52996T^*)} + \frac{1.76474}{exp(3.89411T^*)}
\end{aligned}
\tag{23}
$$

At the high temperatures of the process, above 1000K, we can do the following approximation:

$$\Omega_{D_{X-m}} \approx \frac{1.06036}{T^{*0.15610}} \tag{24}$$

468 Hence D_{ij} is approximatively proportional to $T^{3/2+0.15610}$ and the ratio of two different diffusiv-
469 ities has a dependence on temperature that can be neglected.

470 ## C. SIMPLIFIED NON ISOTHERMAL MODEL - DILUTED CASE

In this part, we are giving arguments to confirm the relationship 6 in the non-isothermal case with
the injection of cold gases. As shown in annex B, the diffusivity ratios does not vary significantly
with temperature. In the diluted case, we write Fick's law for gases for a specie X:

$$
\begin{aligned}
J_X^{mol} &= -D_X c \frac{\partial x_X}{\partial z} \\
&= -\frac{D_X}{RT} \frac{\partial P_X}{\partial z}
\end{aligned}
\tag{25}
$$

471 The linear relationship 19 that was due to the appearance of silica in the diluted case then
472 becomes:

$$\left(p_{O_2}^{eff} - p_{Si}^{eff}\right) = A \int_0^z \frac{T(z')}{D_{O_2}(z')}dz' + B \tag{26}$$

---

[4]1687 K is the fusion temperature of silicon according to the SGTE-SGPS database [28]

We then obtain the relationship:

$$J_{\mathrm{Si}} \approx \frac{\frac{1}{2}\Psi_{\mathrm{H_2O}}P_{\mathrm{H_2O}}^0 + \frac{1}{2}\Psi_{\mathrm{SiO}}P_{\mathrm{SiO}}^{surf}}{R\int_0^\delta \frac{T(z')}{D_{\mathrm{O_2}}(z')}dz'} \tag{27}$$

In the case without aerosols, we would have:

$$J_{\mathrm{Si}} \quad = \frac{\Psi_{\mathrm{H_2O}}P_{\mathrm{H_2O}}^0}{\int_0^\delta RT(z)/D_{\mathrm{O_2}}(z)dz} \tag{28}$$

We then find the relationship 4 again. The negative temperature gradient in cold gas does however modify the equilibrium constant, favoring the formation of silica aerosols and diminishing the partial pressures of reactive species SiO(g) and H$_2$O(g) relatively to the isothermal case. This is going to diminish P_{SiO}^{surf} relatively to the isothermal case, thus strengthening the approximation of equation 6 relatively to the isothermal case.

In the present model, we have not accounted for the effect of thermodiffusion. The thermodiffusion effect increases the diffusion rate of lighter molecules towards the heated surface compared to heavier molecules. [30]. In the cold gas case, this would lead SiO(g) (which is heavier than H$_2$O(g), H$_2$(g) and Ar(g)) to diffuse more rapidly from the heated surface, which would lower the concentration of SiO(g) at the surface relatively to the present model. Hence, this makes the approximation 4 that the formation of silica aerosol reduces the outflow of silicon by a factor two even more accurate.

References

[1] J. Safarian, G. Tranell, and M. Tangstad: *Energy Procedia*, 2012, vol. 20, pp. 88–97.

[2] Y. Delannoy, M. Heuer, E. Øvrelid, and S. Pizzini: *3 Conventional and Advanced Purification Processes of MG Silicon*, CRC press. 2017.

[3] Ø. S. Sortland: *Boron removal from silicon by steam and hydrogen.* PhD thesis, NTNU,Norway, 2015.

[4] Altenberend: *Kinetics of the plasma refining process of silicon for solar cells experimental study with spectroscopy.* PhD thesis, Grenoble-INP,France, 2012.

[5] Ø. S. Sortland and M. Tangstad: *Metallurgical and Materials Transactions E*, 2014, vol. 1, pp. 211–225.

[6] J. Altenberend, G. Chichignoud, and Y. Delannoy: *Metallurgical and Materials Transactions E*, 2017, vol. 4, pp. 41–50.

[7] M. Vadon, Y. Delannoy, and G. Chichignoud: *Metallurgical and Materials Transactions B*, pp. 1–8.

[8] A. Fluent: *Canonsburg, PA, USA: ANSYS Inc*, 2012.

[9] S. B. Pope: 1997.

[10] Y. Delannoy, C. Alemany, K.-I. Li, P. Proulx, and C. Trassy: *Solar energy materials and solar cells*, 2002, vol. 72, pp. 69–75.

20

[11] D. Pelletier, Y. Delannoy, and C. Trassy: *High Temperature Material Processes (An International Quarterly of High-Technology Plasma Processes)*, 2010, vol. 14.

[12] M. Majchrzak, J. Altenberend, Y. Delannoy, and G. Chichignoud: *Bulletin of the American Physical Society*, 2010, vol. 55.

[13] D. Pelletier: *Modélisation de la cinétique chimique dans les plasmas inductifs.* PhD thesis, 2006.

[14] J.-G. Lacombe: *Transferts radiatifs dans les plasmas thermiques.* PhD thesis, Thèse INP Grenoble, 2008., 2008.

[15] J. Degoulange: *Purification et caractérisations physico-chimiques et électriques de silicium d'origine métallurgique destiné à la conversion photovoltaïque.* PhD thesis, Institut National Polytechnique de Grenoble-INPG, 2008.

[16] C. Alemany, C. Trassy, B. Pateyron, K.-I. Li, and Y. Delannoy: *Solar energy materials and solar cells*, 2002, vol. 72, pp. 41–48.

[17] M. W. Chase: *JANAF thermochemical tables, by Chase, MW Washington, DC: American Chemical Society; New York: American Institute of Physics for the National Bureau of Standards, c1986.. United States. National Bureau of Standards.*, 1986, vol. 1.

[18] M. Page: *The Journal of Physical Chemistry*, 1989, vol. 93, pp. 3639–3643.

[19] S. Gorokhov, L.N.and Polisadin and A. Emelyanov: *XII AllUnion Conference on calorimetry and chemical thermodynamics,1991,Krasnoyarsk,Theses of the reports*, 1991, p. 58.

[20] N. S. Jacobson and D. L. Myers: *The Journal of Physical Chemistry B*, 2011, vol. 115, pp. 13253–13260.

[21] L. V. G. I. V. V. C. B. Alcock: *Thermodynamic properties of individual substances. Vol. 3, Elements B, Al, Ga, In, Tl, Be, Mg, Ca, Sr, Ba and their compunds, Part 1, Methods and computation*, Reading, Massachusetts: Boca Raton : CRC. 1994.

[22] I. Ansara, A. Dinsdale, and M. Rand: *Office for Official Publications of the European Communities*, 1998.

[23] R. A. Svehla:, "Estimated viscosities and thermal conductivities of gases at high temperatures" tech. rep., National Aeronautics and Space Administration. Lewis Research Center, Cleveland, 1962.

[24] S. Schnurre, J. Gröbner, and R. Schmid-Fetzer: *Journal of Non-Crystalline Solids*, 2004, vol. 336, pp. 1–25.

[25] M. Ratto, E. Ricci, E. Arato, and P. Costa: *Metallurgical and Materials Transactions B*, 2001, vol. 32, pp. 903–911.

[26] A. V. Plyasunov: *Geochimica et Cosmochimica Acta*, 2011, vol. 75, pp. 3853–3865.

[27] E. Opila: *Calphad*, 2016, vol. 55, pp. 32–40.

[28] C. Bale, P. Chartrand, S. Degterov, G. Eriksson, K. Hack, R. B. Mahfoud, J. Melançon, A. Pelton, and S. Petersen: *Calphad*, 2002, vol. 26, pp. 189–228.

[29] R. Bird, W. Stewart, and E. Lightfoot: *Transport Phenomena*, Wiley. Wiley International edition, 2007.

[30] A. FLUENT: *Ansys Inc.*

[31] D. Baulch, C. Bowman, C. Cobos, R. Cox, T. Just, J. Kerr, M. Pilling, D. Stocker, J. Troe, W. Tsang, *et al.*: *Journal of physical and chemical reference data*, 2005, vol. 34, pp. 757–1397.

[32] C. Park: *Journal of Thermophysics and Heat Transfer*, 1989, vol. 3, pp. 233–244.

[33] J. Park, E. Pfender, and C. Chang: *Plasma Chemistry and Plasma Processing*, 2000, vol. 20, pp. 165–181.

[34] M. L RIGHTLEY and F. Williams: *Combustion Science and Technology*, 1997, vol. 125, pp. 181–200.

[35] P. Saxena and F. A. Williams: *Combustion and Flame*, 2006, vol. 145, pp. 316–323.

[36] A. A. Konnov: *Combustion and flame*, 2008, vol. 152, pp. 507–528.

LIST OF FIGURES

LIST OF TABLES

Table 1: *Varying experimental parameters and results for the Q_X series (source: Sortland et al.[5]).*

Gas Flow Rate	Q (l_n/min)	Time (min)	Initial [B] (ppmw)	Final [B] (ppmw)	$k_t \pm \sigma$ ($\mu m/s$)
Q_4	4.00	60.0	109 ± 7	4.5 ± 0.3	19.0 ± 0.8
Q_6	6.00	60.0	80 ± 11	2.4 ± 0.2	21.0 ± 0.3
Q_10	10.00	60.0	62 ± 4	0.8 ± 0.02	33.7 ± 1.5
Q_12	12.00	36.5	60 ± 6	0.8 ± 0.03	41.5 ± 2.1
Q_14	14.00	36.0	74 ± 10	0.8 ± 0.06	44.6 ± 2.9
Q_16a	16.00	35.7	36 ± 2	0.7 ± 0.03	40.8 ± 1.7
Q_16b	16.00	37.4	80 ± 3	0.6 ± 0.03	51.1 ± 1.8

Table 2: *Varying experimental parameters for the H_2O_X series (source: Sortland et al.[3]).*

"H2O" Experiments	P_{H2O} (bar)
H2O_15	0.15
H2O_20	0.197
H2O_25	0.251
H2O_30	0.300
H2O_35	0.351
H2O_40	0.399

Table 3: *Parameters for the plasma experiment by Altenberend [4] with comparison to the conditions for the plasma in Degoulange [15].*

	Power (KW)	Temperature Si(l) (K)	Flow Ar (Nm3/h)	Flow H2 (Nm3/h)
Alt [4]	38.00	1687	7.33	0.31
Deg [15]	28.00	1950	5	0

	Flow O2 (Nm3/h)	Diameter Target (mm)	Distance Torch - Surface (mm)	Distance Torch- Injector (mm)
Alt [4]	0.06	120	60	67
Deg [15]	0.038	320	100	

572

Table 4: *Geometrical parameters for the plasma Experiment (source: Altenberend [6]).*

	Si(l) surface area A (m^2)	Silicon Mass m_{Si}(kg)	Silicon Volume V (m^3)	Area /Volume Ratio m^{-1}
Alt [4]	0.0113	2.9	0.00135	8.34
Deg [15]	0.020		0.0006	33

573

Table 5: *Estimates of P_{SiO}^{surf} at different temperatures for $P_{H_2} = 1$ bar.*

T	P_{SiO}^{surf} (bar)
1683K	0.001
1773K	0.0025
1973K	0.016

Table 6: *Diffusivities from Svehla [23].*

Molecule	σ	ϵ/k d
SiO	3.374	569
H2O	2.641	809.1
H2	2.827	59.7
Ar	3.542	93.3

Table 7: *Data for $Si(OH)_4(g)$ from SGTS-SGPE database using Plyasunov et al. [26].*

	DH(298.15) (J/mol)	S(298.15) (J/mol-K)	C(i)	P(i)	C(i)	P(i)	Cp (K)
1	-1340680.00	347.780000	37.949080	0	0.36664390	1	298 - 400
1			-159690.10	-2	-3.37740400E-04	2	298 - 400
2			140.68790	0	1.82143200E-02	1	400 - 1200
2			-2970717.0	-2	1.02132400E-06	2	400 - 1200
3			136.88860	0	2.94423700E-02	1	1200 - 2400
3			-4945980.0	-2	-4.74436200E-06	2	1200 - 2400
4			180.37840	0	3.46074200E-03	1	2400 - 4000
4			-42965010.	-2	-3.23079100E-07	2	2400 - 4000

Table 8: *Standard enthalpies and entropies of formation of species at* 298 K *used for the plasma model [NIST-Baulch, 2005] [31].*

Chemical species	$\Delta_f H^0(298.15K)$ (kJ/mol)	$S^0(298.15K)$ (J/mol/K)
Ar	0	154,72
Ar+	1526,77	166,4
O2	0	205,03
O	249,16	161,06
O+	156,87	154,96
H2	0	130,68
H	217,97	114,72
H+	153,62	108,95
OH	37,17	183,71
H2O	-241,82	188,84
e-	0	208,58

Table 9: *Kinetic parameters for the plasma Ar-O_2-H_2. M represents a catalytic specie.*

Chemical reactions	A (cm3/mol/s)	n	Ea (kJ/mol)	ref
1. $Ar + M \rightarrow Ar + +e- +M$	3,06E+013	0,5	1120	[Hoffert, 1967]
2. $O2 + M \rightarrow 2O + M$	2,00E+021	-1,5	490	[Park, 2000]
3. $O2 + e- \rightarrow O + O + +2e-$	3,19E+014	0,9	493,55	Park, 1989 [32]
4. $O + e- \rightarrow O + +2e-$	3,91E+033	-3,78	1320	Park,2000 [33]
5. $H2 + M \rightarrow 2H + M$	2,23E+012	0,5	390	Park,2000 [33]
6. $H + e- \rightarrow H + +2e-$	1,51E+031	-3	1313,7	Park,2000 [33]
7. $O + H2 \rightarrow OH + H$	5,06E+004	2,7	26,3	Rightley,1997 [34]
8. $H + O2 \rightarrow OH + O$	3,52E+016	-0,7	71,4	Rightley,1997 [34]
9. $O + H + M \rightarrow OH + M$	4,71E+018	-1	0	Saxena, 2006 [35]
10. $H + OH + M \rightarrow H2O + M$	4,00E+022	-2	0	Saxena, 2006 [35]
11. $OH + OH \rightarrow H2O + O$	3,34E+004	2,42	-8,06	Konnov, 2008 [36]
12. $H2 + OH \rightarrow H2O + H$	1,17E+009	1,3	15,2	Rightley,1997 [34]

Table 10: *The concentration of catalytic species is estimated with these rules.*

Pour 1	[M] = 0,444E-7 [Ar] + 1 [e-]
Pour 2	[M] = 5 [O] + 5 [O+] + 5 [H] + 5 [H+] + 45,19 [e-] + 5 [Ar] + 1 [others]
Pour 5	[M] = 3,848 [H+] + 1155,5 [H] + 18,4 [H2O] + 14,75 [e-] + 1 [others]
Pour 9	[M] = 0.75 [Ar] + 2.5 [H2] + 12 [H2O] + 1 [others]
Pour 10	[M] = 0.38 [Ar] + 2.5 [H2] + 12 [H2O] + 1 [others]